APPLIED FUZZY LOGIC CONTROLS FOR IMPROVING DYNAMIC RESPONSE OF INDUCTION MACHINES

by

Altaf Ahmad Syed

Submitted in partial Fulfillment of the Requirements

for the Degree of

Master of Science in Engineering

in the

Electrical and Computer Engineering

Program

YOUNGSTOWN STATE UNIVERSITY

Youngtown, Ohio

August, 2008

APPLIED FUZZY LOGIC CONTROLS FOR IMPROVING

DYNAMIC RESPONSE OF INDUCTION MACHINES

Altaf Ahmad Syed

I hereby release this thesis to the public. I understand that this thesis will be made available from the OhioLINK ETD Center and the Maag Library Circulation Desk for public access. I also authorize the University or other individuals to make copies of this thesis as needed for scholarly research.

Signature:

_____

Altaf Ahmad Syed, Student Date

Approvals:

_____

Dr. Jalal Jalali, Thesis Adviser Date

_____

Dr. Philip Munro, Committee Member Date

_____

Dr. Faramarz Mossayebi, Committee Member Date

_____

Peter J. Kasvinsky, Dean of Graduate Studies & Research Date

ABSTRACT

This thesis presents a novel approach in control systems for improving the dynamic response of the induction machine. This approach leads to a better and improved control of the torque and current response of the induction machine when compared to the classical proportional-integral (PI) type controller with de-coupling terms. Mismatches in the actual parameters and the estimated parameters of the induction machine occur for several reasons such as: incorrect parameter estimation, changes in stator and rotor inductance due to saturation, stator and rotor resistance varying with temperature, etc. Under the classical approach, the de-coupling errors resulting from the parameter mismatches can become very large at higher machine rotational speeds. Under such conditions, the classical approach results in poor dynamic control of the torque and current response of the induction machine. Therefore, an advanced fuzzy logic controller is presented as a better alternative to the classical controller. The fuzzy logic-based *d-q* controller, based on its non-linear approach, provides robust control of the torque and current response of the induction machine even in the presence of mismatched parameters. Furthermore, the performance of the fuzzy logic controller is not dependent on the machine rotational speed. Using MATLAB-SIMULINK tools, the performance of the fuzzy controller is evaluated with mismatched machine parameters at various machine rotational speeds. The results show that the use of the fuzzy logic controller offers a superior control of the torque and current response of the induction machine, independent of the motor rotational speed when compared with the use of the classical controller.

ACKNOWLEDGEMENTS

I would like to acknowledge the great support Dr. Jalal Jalali provided me during my studies at Youngstown State University. I would also like to thank Dr. Philip Munro, Dr. Robert Foulkes and Dr. Duane Rost for the knowledge they passed onto me during my undergraduate studies at Youngstown State University. Finally, I would like to thank all my friends and family for providing the support I needed during my graduate studies.

TABLE OF CONTENTS

LIST OF FIGURES

LIST OF TABLES

1. INTRODUCTION

A large percentage of current electrical machines found in industry are squirrel cage AC induction machines. These machines are widely used in industrial applications because they are less expensive and more rugged and reliable than DC motors [1]. The widespread use of these machines will continue due to their versatility, dependability and low cost. In the past, squirrel cage induction machines were limited to constant speed applications, and were operated from a fixed sinusoidal supply. The development of high power switching devices in the last decade has accelerated the growth in the market for variable speed drive systems incorporating AC induction machines and variable speed drives [1]. The robust construction of the squirrel cage induction machine together with high excitation frequency capabilities of the VSD (variable speed drive) allow for the operation of induction machines at very high rotational speeds [1].

In high performance applications that require precision speed and/or torque control, induction machines are frequently used [1]. Servo motor drives and spindle motor drives are examples of applications requiring precision speed control whereas electric vehicle drive systems require robust torque control.

An induction machine connected to a mechanical load and operated from a variable frequency drive, along with associated feedback sensors, constitutes an electric machine drive system [1]. In order to provide variable speed capability and control for an induction machine, a variable speed drive must include a variable frequency source (inverter) and a control system [1]. Inverters are DC to AC converters, whose power is supplied by a rectifier fed from the AC power line. Rectifiers draw distorted, non-

sinusoidal currents; hence passive or active filters are used on the input side to reduce the low frequency harmonic content in the supply current [1]. The control system of variable speed drives usually consists of microcontrollers, microprocessors and digital signal processors (DSPs) [1]. For precision control of induction machines, high performance control systems are usually employed. Such control systems use sensors of voltage, current, speed or position for feedback and usually require some knowledge of the induction machine parameters at steady-state.

Although induction machines have several advantageous characteristics such as simplicity, ruggedness and low cost, they also exhibit non-linear and time-varying dynamic behaviors [2]. When compared to a DC machine, the control system required for controlling the induction machine behavior is complicated, since the field and torque-producing components of the stator current are linked [1]. In order to achieve precise control of induction machines, it is necessary to control these two components of the stator current independently.

In the last decade, with the development of faster microcontrollers and DSPs, the field-oriented (vector) control technique has created a renaissance in modern high-performance control of pulse width modulated (PWM) inverter fed induction machines [1]. Today, field-oriented (vector) control is the most popular control method used in high performance industrial applications using the induction machine. Hasse in 1969, and Blaschke in 1972 first proposed the concept of field-orientation [1]. The objective of the field-orientation is to make the induction machine behave like a separately excited DC machine where torque and flux can be independently controlled [1][3]. Vector control schemes have allowed the induction machine to achieve torque control

performance similar to that of a separately excited DC machine and have led to the replacement of the DC machine by the induction machine in many high performance applications [3]. Furthermore, it has also resulted in faster transient response of the induction machine due to de-coupled control of torque and rotor flux.

There are two types of vector control methods; direct and indirect field-orientation. The direct field-orientation (DFO) method uses direct measurement of the air-gap flux vector by means of special search coils, or Hall Effect sensors embedded in the air gap. Even though this method results in accurate control, the application of this method is very limited, as induction machines equipped with flux measuring sensors are required [1]. In spite of its accuracy, this method degrades the motor's main advantages of mechanical simplicity and ease of maintenance [1]. In the indirect field-orientation (IFO), the rotor flux is estimated from the stator current vector, rotor speed and the machine estimated parameters. The drawback of this method is that it is sensitive to the variations in the induction machine parameters [4].

The objective of this research is to design a robust controller employing indirect field-oriented control to improve the dynamic control of the induction. The classical proportional-integral (PI-type) controller with de-coupling compensation method is most commonly used to implement the indirect field-oriented control due to its simple control algorithm and easy implementation [5][6]. This approach is based on a fixed model of the induction machine and requires accurate values of machine parameters. When there is a mismatch between the estimated induction machine parameters and the actual parameters, the performance of classical controller can deteriorate significantly. In applications requiring robust torque control, the sensitivity of the classical controller to

the machine parameter variations is even higher. Impact of parameter variations on various vector control schemes has been studied in great detail in the past [7][8] [9] [10]. The consequence of parameter mismatch between the values used in the controller and those in the machine is that the actual rotor flux position does not coincide with the position assumed by the controller. This leads to a loss of de-coupled flux and torque control of the induction machine. Performance of the controller therefore deteriorates from the desired. The problem of loss of de-coupled flux and torque control is even more profound at high-speed operation of the induction machine [4][5].

Various methods have been suggested to address this concern [4][5][7][11]. One such method is to provide the controller with accurate induction machine parameter values at all times. This means that the controller has to account for the several variables such as: changes in motor temperature, changes in the stator and rotor inductance due to saturation and high frequency, rotor skin effect, etc. Using classical methods, it is very difficult and computationally intensive to design a high performance induction machine drive system that takes all parameter variations into account. Other methods include use of internal model controller or additional PI controllers to compensate for the parametric variation errors. The method requiring an accurate model of induction machine is not practical while the use of internal model controller is not suited for variable speed operation [4].

The research presented in this study uses fuzzy logic-based non-linear approach for the design of a robust induction machine control system. The fuzzy logic control is a non-linear control technique and it allows for the control of non-linear system such as

induction machines. There are three main characteristics of a fuzzy logic controller [2][12]:

1) The fuzzy controller is a linguistic controller and does not require a precise and accurate mathematical model of the controlled object.
2) The fuzzy logic controller is an ideal flexible non-linear type controller as it can overcome the influence of non-linear variations.
3) The fuzzy logic controller provides robust control as it is insensitive to parametric variations of the controlled process.

The application of fuzzy logic in the control of induction machines has been well-documented [1][8][9][13][14][15]. It has been shown that the performance of the induction machine system as well as robustness to parameter variations can be improved by the use of fuzzy logic controller design [2][14][16]. However, these fuzzy logic-based designs exist for controlling induction machines to a desired speed, and no effective control system yet exists for the torque control of induction machine. In this thesis, an advanced fuzzy logic controller for an indirect field-oriented induction machine is presented. This fuzzy logic controller improves the torque and current response of induction machine and is robust to parameter variations. This advanced fuzzy logic controller can be used in high performance applications such as automotive drive systems, dynamometer test stands, high-speed spindles, etc.

In order to design an effective fuzzy logic controller and evaluate its performance, a detailed model of the induction machine and the induction control system is presented. Additionally, by the use of MATLAB-SIMULINK, extensive simulations of the complete system were performed to validate the robustness of the fuzzy controller. Using

MATLAB-SIMULINK, the performance of the fuzzy controller is evaluated with mismatched induction machine parameters under different operating conditions such as: step change in load in speed control mode, and step change in torque command. The simulation results from the fuzzy controller were then compared to that of the classical controller. The results show the superiority of the proposed advanced fuzzy controller over the classical controller in presence of the parameter mismatch and at high speeds. Results validate the robustness and effectiveness of the proposed fuzzy logic controller for controlling the dynamic torque and current response of the induction machine system.

This research is structured as follows:

- Chapter 2 provides the background information on the space vector transformations (*d-q* transformation), the dynamic equivalent circuit of the squirrel cage induction machine and the voltage source inverter model.
- In Chapter 3, the scalar and vector control techniques available for control of induction machines along with their advantages and disadvantages are presented. Furthermore, a detailed plant model of the induction machine for indirect field-oriented control (vector control) is created for use with MATLAB-SIMULINK.
- In Chapter 4, a fuzzy logic-based induction machine control system is presented for effective control of induction machines. The design of the fuzzy logic-based *d-q* controller used in this control system is also detailed in this chapter. Furthermore, the complete model of the fuzzy logic-based induction machine control system is implemented using MATLAB-SIMULINK.
- In Chapter 5, a complete simulation environment consisting of the operator inputs model, the fuzzy logic-based induction machine control system and the induction

machine plant model is presented. Using MATLAB-SIMULINK, various simulations of the complete induction machine system are performed using the fuzzy controller and the classical controller. The simulation results are then presented which compare the performance of the fuzzy controller to that of the classical controller.

- Chapter 6 provides the conclusions drawn from this research. Potential areas for further research that could result in further improvements of the fuzzy logic controller are also presented in this chapter.

2. DERIVATION OF INDUCTION MACHINE SYSTEM EQUATIONS

2.1. INTRODUCTION

DC motors have been traditionally used in the applications requiring high dynamic performance and precision speed and torque control. Examples of such applications include: high performance dynamometer systems, elevator motors, spindle drive motors and servomotors. Even though induction machines have been commonly used in industrial settings, their application was mostly limited to constant speed applications. With the recent advances in power electronics, several classes of variable speed drives have been developed that provide the AC induction machine with an edge over the DC machine. Because of simple, rugged and robust design of the induction machine, they can be operated at much higher speeds compared to the DC machine. The advances in the power electronics and digital control systems make induction machines an interesting solution for a wide range of applications. This increased interest in the induction machine has even led to its use in the automotive industry for fuel cell, hybrid-electric, and electric vehicles.

The other type of electric machines quickly gaining in popularity is AC permanent magnet machines. The most important benefits, which are expected when introducing permanent magnet machines, are lower losses and a higher torque density. Among the drawbacks are comparatively higher cost, increased temperature sensitivity, relatively complex controls and the need for sensors of flux. For high-speed capabilities, a fiber glass band is required for the retention of the surface mounted magnets [17].

Although the magnet-retaining band prevents the magnets from detaching, it degrades the heat dissipation of the magnets [17]. The induction machine on the other hand has a robust rotor construction, which makes it suitable for high-speed applications. The induction machine is also capable of providing a wider constant horsepower (HP) range compared to an AC permanent magnet machine [1][4][17]. And with new innovative cooling techniques, the new generation of induction machines also offer relatively higher torque density as well as higher efficiency. With the induction machines offering so many advantages over their rivals, their use in the industrial settings will continue to increase.

In an application where the goal is to optimize the system dynamic response and achieve high dynamic performance, a robust controller design is essential. Because of the non- linear nature of the induction machine, the controller must be able to control the non-linear behavior and provide a fast and accurate response. In this chapter, background information is provided on the concept of space vector transformations, induction machine equivalent circuit, and the voltage source inverter. The focus of this chapter is on deriving the dynamic equations for the induction machine and related components. The dynamic equations can then be used create a dynamic model of the induction machine.

2.2. INDUCTION MACHINE SYSTEM

Figure 2.1 shows the model of an AC induction machine system. The block diagram in Figure 2.1 shows the basic blocks involved in an induction machine system.

The five basic blocks are; voltage rectifier, input DC supply, inverter module, controller and an induction machine. The AC power source is typically a three-phase, 230V or 460V system. A rectifier is used to convert the three-phase AC voltage to provide the DC supply for the inverter. The input DC supply is usually placed in the form of a capacitor bank between the rectifier and the inverter. The inverter module along with the

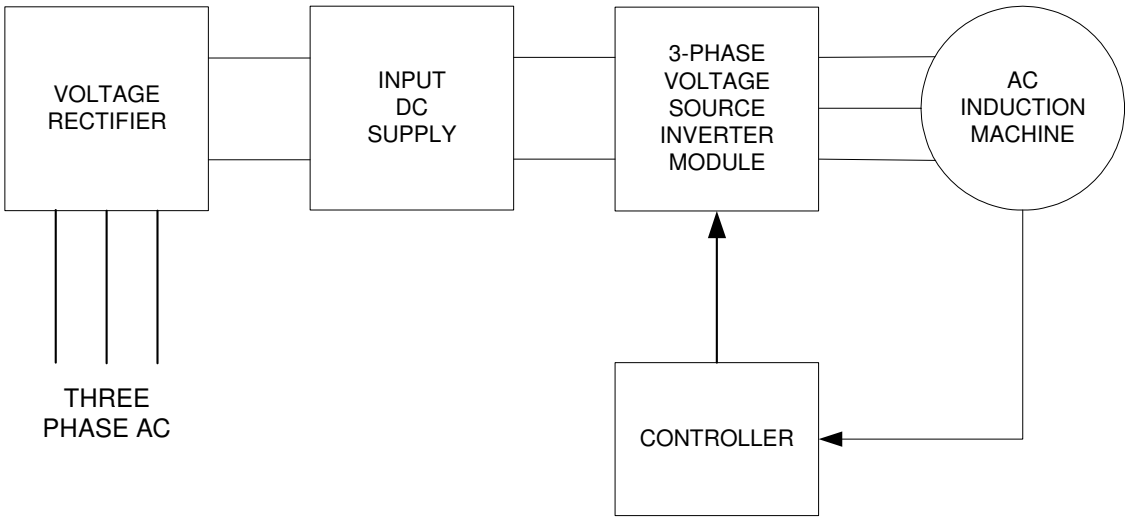

Figure 2.1. Block diagram of induction machine system

inputs from the controller converts the DC supply voltage (V_{DC}) to three-phase AC voltage. This three-phase AC voltage is sometimes optionally filtered and then drives the induction machine. As the inputs to the induction machine are three-phase AC voltages, the idea of a rotating direct and quadrature-axis frame (*d-q* frame) is introduced to transform the three-phase AC vectors into DC signals.

2.3. SPACE VECTOR TRANSFORMATIONS

Space vectors of three-phase variables, such as voltage, current, or flux, are very convenient for analysis and control of the induction machine system. Consider three-phase arbitrary vectors, $\hat{\Re}_{as}, \hat{\Re}_{bs}, \hat{\Re}_{cs}$, whose total vector sum, $\hat{\Re}_s$, can be represented as follows [1][3]:

$$\hat{\Re}_s = \hat{\Re}_{as} + \hat{\Re}_{bs} + \hat{\Re}_{cs} = \Re_{as} + \Re_{bs} e^{j\frac{2}{3}\pi} + \Re_{cs} e^{j\frac{4}{3}\pi} \tag{2.1}$$

Since $e^{j\frac{2}{3}\pi} = -\frac{1}{2} + j\frac{\sqrt{3}}{2}$, and $e^{j\frac{4}{3}\pi} = -\frac{1}{2} - j\frac{\sqrt{3}}{2}$, eq. (2.1) can be rewritten as follows:

$$\hat{\Re}_s = \Re_{as} - \frac{1}{2}\Re_{bs} - \frac{1}{2}\Re_{cs} + j\left(\frac{\sqrt{3}}{2}\Re_{bs} - \frac{\sqrt{3}}{2}\Re_{cs}\right) \tag{2.2}$$

As an example, the sum of three-phase currents is zero, which implies that one of the currents can be eliminated and therefore one degree of freedom can be reduced and space vectors can be represented in an equivalent two-phase space vectors. Using such an analogy the sum of the vectors can be represented as follows:

$$\hat{\Re}_s = \Re^s_{ds} + j\Re^s_{qs} = \Re_{as} - \frac{1}{2}\Re_{bs} - \frac{1}{2}\Re_{cs} + j\left(\frac{\sqrt{3}}{2}\Re_{bs} - \frac{\sqrt{3}}{2}\Re_{cs}\right) \tag{2.3}$$

where superscript *s* denotes a stationary direct-quadrature axis (*d*-*q*) frame. Equation (2.3) explains the *abc* to dq^s transformation. The transformation can be rewritten as follows [1]:

$$\begin{bmatrix} \Re^s_{ds} \\ \Re^s_{qs} \end{bmatrix} = \begin{bmatrix} 1 & -\frac{1}{2} & -\frac{1}{2} \\ 0 & \frac{\sqrt{3}}{2} & -\frac{\sqrt{3}}{2} \end{bmatrix} \begin{bmatrix} \Re_{as} \\ \Re_{bs} \\ \Re_{cs} \end{bmatrix} \tag{2.4}$$

and

$$\begin{bmatrix} \Re_{as} \\ \Re_{bs} \\ \Re_{cs} \end{bmatrix} = \begin{bmatrix} \frac{2}{3} & 0 \\ -\frac{1}{3} & \frac{1}{\sqrt{3}} \\ -\frac{1}{3} & -\frac{1}{\sqrt{3}} \end{bmatrix} \begin{bmatrix} \Re^{s}_{ds} \\ \Re^{s}_{qs} \end{bmatrix} \tag{2.5}$$

Transformations in equations (2.4) and (2.5) apply to all three-phase variables of any three-phase system, which add up to zero.

In a balanced system, where the sum of all the three vectors is zero, the magnitude of $\hat{\Re}_s$ is $\frac{3}{2}$ higher than the magnitude (peak value), $\Re_{as}$, of phase vectors. Hence the equation (2.4) can be multiplied by $\frac{2}{3}$ and equation (2.5) can be multiplied by $\frac{3}{2}$.

The final transformation can therefore be written as follows [1][3]:

$$\begin{bmatrix} \Re^{s}_{d} \\ \Re^{s}_{q} \end{bmatrix} = \frac{2}{3} \begin{bmatrix} 1 & -\frac{1}{2} & -\frac{1}{2} \\ 0 & \frac{\sqrt{3}}{2} & -\frac{\sqrt{3}}{2} \end{bmatrix} \begin{bmatrix} \Re_{a} \\ \Re_{b} \\ \Re_{c} \end{bmatrix} = \begin{bmatrix} \frac{2}{3} & -\frac{1}{3} & -\frac{1}{3} \\ 0 & \frac{1}{\sqrt{3}} & -\frac{1}{\sqrt{3}} \end{bmatrix} \begin{bmatrix} \Re_{a} \\ \Re_{b} \\ \Re_{c} \end{bmatrix} = T \begin{bmatrix} \Re_{a} \\ \Re_{b} \\ \Re_{c} \end{bmatrix} \tag{2.6}$$

and,

$$\begin{bmatrix} \Re_{a} \\ \Re_{b} \\ \Re_{c} \end{bmatrix} = \frac{3}{2} \begin{bmatrix} \frac{2}{3} & 0 \\ -\frac{1}{3} & \frac{1}{\sqrt{3}} \\ -\frac{1}{3} & -\frac{1}{\sqrt{3}} \end{bmatrix} \begin{bmatrix} \Re^{s}_{d} \\ \Re^{s}_{q} \end{bmatrix} = \begin{bmatrix} 1 & 0 \\ -\frac{1}{2} & \frac{\sqrt{3}}{2} \\ -\frac{1}{2} & -\frac{\sqrt{3}}{2} \end{bmatrix} \begin{bmatrix} \Re^{s}_{d} \\ \Re^{s}_{q} \end{bmatrix} = T' \begin{bmatrix} \Re^{s}_{d} \\ \Re^{s}_{q} \end{bmatrix} \tag{2.7}$$

where,

$$T = \begin{bmatrix} \frac{2}{3} & -\frac{1}{3} & -\frac{1}{3} \\ 0 & \frac{1}{\sqrt{3}} & -\frac{1}{\sqrt{3}} \end{bmatrix} \tag{2.8}$$

and

$$T' = \begin{bmatrix} 1 & 0 \\ -\frac{1}{2} & \frac{\sqrt{3}}{2} \\ -\frac{1}{2} & -\frac{\sqrt{3}}{2} \end{bmatrix} \tag{2.9}$$

2.4. THREE-PHASE VOLTAGE SOURCE INVERTER

In this section, a three-phase voltage source inverter module is modeled in detail, which converts the DC source voltage to three-phase AC voltage using switching control signals. Figure 2.2 shows a detailed model, which contains ideal switches and diodes [1][18]. Control inputs (S_a, S_b, S_c) are switching functions of time {0,1}.

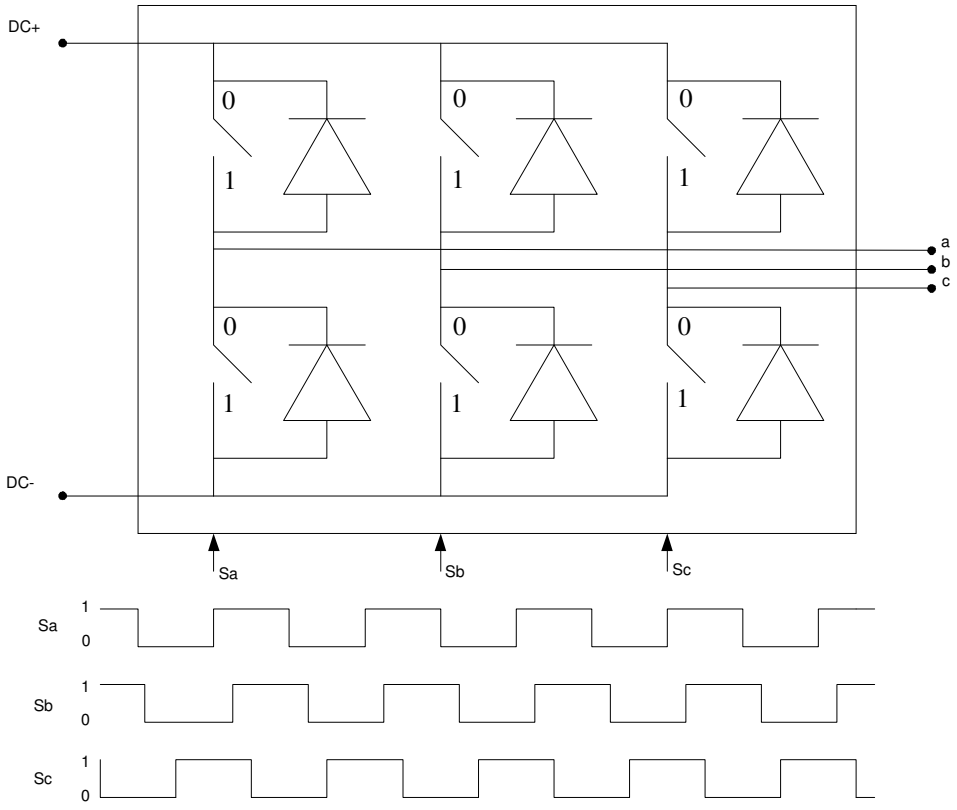

Figure 2.2. VSI Switching model

The control inputs (S_a, S_b, S_c) switch (0 for open position and 1 for closed position) at different intervals or average duty cycles (d_a, d_b, d_c), to produce an average three-phase AC signal. Therefore the average model can be written as follows:

$$\begin{bmatrix} V_a \\ V_b \\ V_c \end{bmatrix} = \begin{bmatrix} d_a \\ d_b \\ d_c \end{bmatrix} kV_{DC} \tag{2.10}$$

where V_a, V_b, and V_c are three-phase AC voltage outputs, considering the Y-connected load, V_{DC} is the DC source voltage, d_a, d_b, and d_c are phase duty cycle of inverter, and k is a constant which depends on the nature of the control signal modulation. A value of ½ is used for k, when the nature of modulation is pure sinusoidal, and a value of $\frac{1}{\sqrt{3}}$ is used when the nature of modulation is source voltage modulation. Line to line voltages and currents can be expressed as follows:

$$\begin{bmatrix} V_{ab} \\ V_{bc} \\ V_{ca} \end{bmatrix} = \begin{bmatrix} V_a - V_b \\ V_b - V_c \\ V_c - V_a \end{bmatrix} \tag{2.11}$$

$$\begin{bmatrix} d_{ab} \\ d_{bc} \\ d_{ca} \end{bmatrix} = \begin{bmatrix} d_a - d_b \\ d_b - d_c \\ d_c - d_a \end{bmatrix} \tag{2.12}$$

$$\begin{bmatrix} V_{ab} \\ V_{bc} \\ V_{ca} \end{bmatrix} = \begin{bmatrix} d_{ab} \\ d_{bc} \\ d_{ca} \end{bmatrix} kV_{DC} \tag{2.13}$$

$$I_{DC} = \begin{bmatrix} d_a & d_b & d_c \end{bmatrix} \begin{bmatrix} I_a \\ I_b \\ I_c \end{bmatrix} \tag{2.14}$$

Equations (2.10) through (2.14) represent the three-phase average model of the voltage source inverter module, and are shown in Figure 2.3 [18].

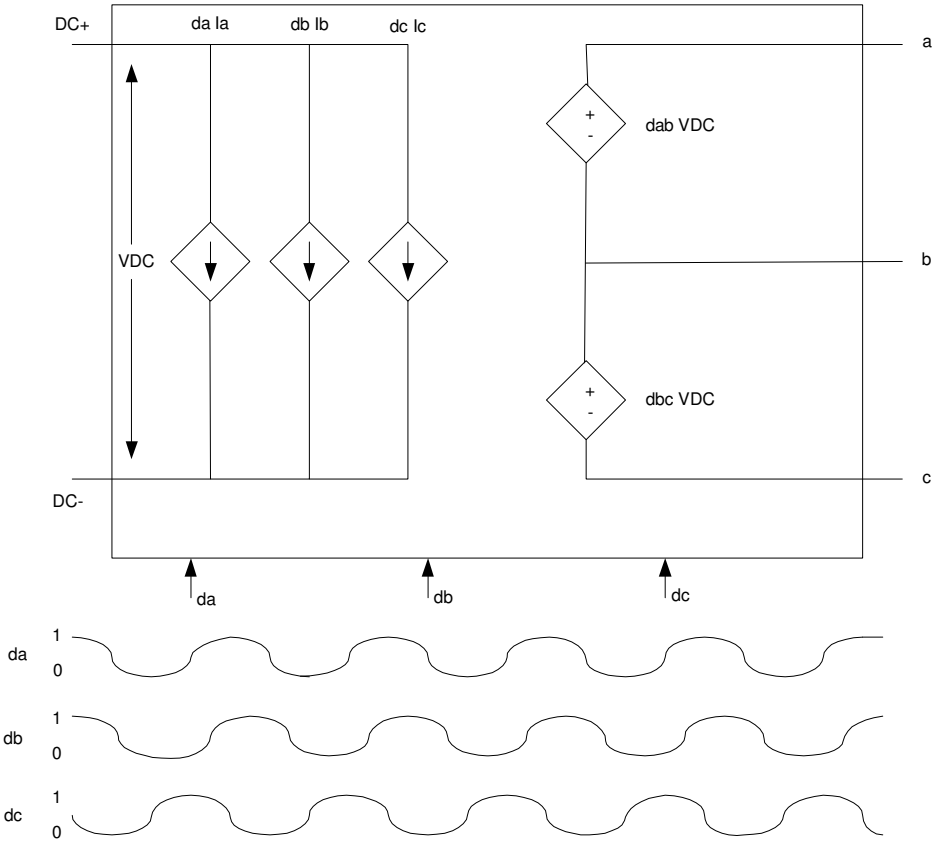

Figure 2.3. Average model of voltage source inverter

The direct and quadrature (*d-q*) components of the phase duty cycle can be defined by applying the transformation in equation (2.6). Using space vector transformations, the phase voltages can be written as follows:

$$\begin{bmatrix} V_d \\ V_q \end{bmatrix} = T \begin{bmatrix} V_a \\ V_b \\ V_c \end{bmatrix} \tag{2.15}$$

Since DC source voltage is used as input, we can define the phase duty cycle *d-q* components as follows:

$$\begin{bmatrix} d_d \\ d_q \end{bmatrix} = T \begin{bmatrix} d_a \\ d_b \\ d_c \end{bmatrix} \tag{2.16}$$

Finally by substituting equations (2.10) and (2.15) into equation (2.16), the relationship between *d-q* voltages and DC source voltage can be written as:

$$\begin{bmatrix} V_d \\ V_q \end{bmatrix} = \begin{bmatrix} d_d \\ d_q \end{bmatrix} kV_{DC} \tag{2.17}$$

The *d-q* to three-phase transformation for currents and duty cycle can be written as follows:

$$\begin{bmatrix} I_a \\ I_b \\ I_c \end{bmatrix} = T' \begin{bmatrix} I_d \\ I_q \end{bmatrix} \tag{2.18}$$

$$\begin{bmatrix} d_a \\ d_b \\ d_c \end{bmatrix} = T' \begin{bmatrix} d_d \\ d_q \end{bmatrix} \tag{2.19}$$

Substituting equations (2.16) and (2.18) into equation (2.14), and after some matrix calculations, the necessary current relationship can be written as follows:

$$I_{DC} = \frac{3}{2} \begin{bmatrix} d_d & d_q \end{bmatrix} \begin{bmatrix} I_d \\ I_q \end{bmatrix} \tag{2.20}$$

In this manner the complete three-phase average voltage source inverter can be modeled in stationary *d-q* coordinate space as shown in Figure 2.4. Finally, the relationship between the DC power and the *d-q* components of voltage and current can be written as follows:

$$P_{DC} = \frac{3}{2} \left(V_d I_d + V_q I_q \right) \tag{2.21}$$

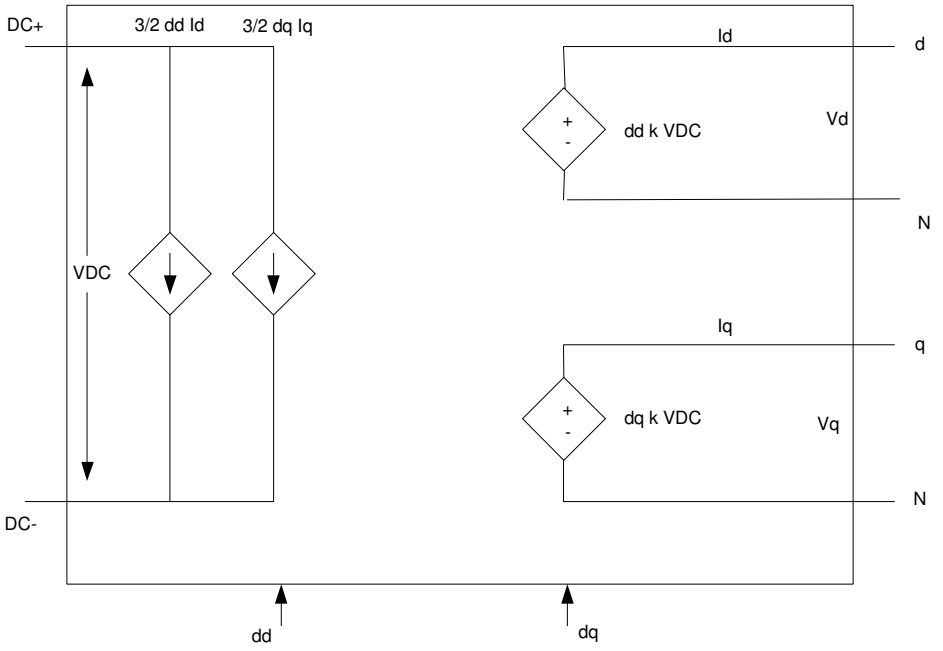

Figure 2.4. VSI average *d-q* model

This model can now be used to determine the DC power required by the inverter module to meet the load demand. In applications such as electric and hybrid electric vehicles, the battery supplies the necessary DC power to the inverter module. In such a case, the implementation of this model can show the amount of DC power consumed by the induction machine and the inverter model to meet the load demand.

2.5. SQUIRREL CAGE INDUCTION MACHINE

The most common form of induction machine used in industrial applications is the squirrel cage induction machine [1]. The other form is wound rotor induction machine. Wound rotor motors are mostly operated on a fixed 60 Hz utility power and are mostly used to limit inrush current and/or achieve high starting torque [1][19]. This

research focuses solely on the squirrel cage induction machine model. The two main components of a squirrel cage induction machine are stator and rotor. The stator has a poly-phase winding set in the slots of the laminated iron core. The rotor does not have any brushes or slip rings. In fact, aluminum or copper bars embedded in the rotor slots form the rotor windings. The rotor bars are short-circuited on each end through end rings. This type of rotor construction looks like a squirrel cage, and is hence called a squirrel cage induction machine. Both the rotor and stator cores are cylindrical. With the slot effects neglected, the air-gap is uniform between the stator and the rotor.

The set of poly-phase currents in the stator windings produces a rotating magnetic field. The windings of the stator are distributed so as to produce a close approximation to a sinusoidal space distribution of magneto-motive force (mmf). The rotor bars experience this field and thus voltage is induced in the rotor conductors. Since these rotor bars are short-circuited, the induce voltage causes current to flow. In turn, the rotor mmf produces a magnetic flux pattern, which also rotates in the air gap at the same speed as that of stator. There is a torque that tends to align the magnetic fields, which results in the rotor moving in the same direction as the magnetic fields. The rotor then accelerates to a speed at which the electromagnetic torque is balanced by the load torque.

Figure 2.5 shows the steady-state equivalent circuit (with core loss neglected) for the analysis and design of induction machine [1][18][19]. In the equivalent circuit, all rotor parameters are referred to the stator. For the equivalent circuit of Figure 2.5, R_s is the stator resistance, R_r is the rotor resistance, L_m is the magnetizing inductance, L_{1s} is the

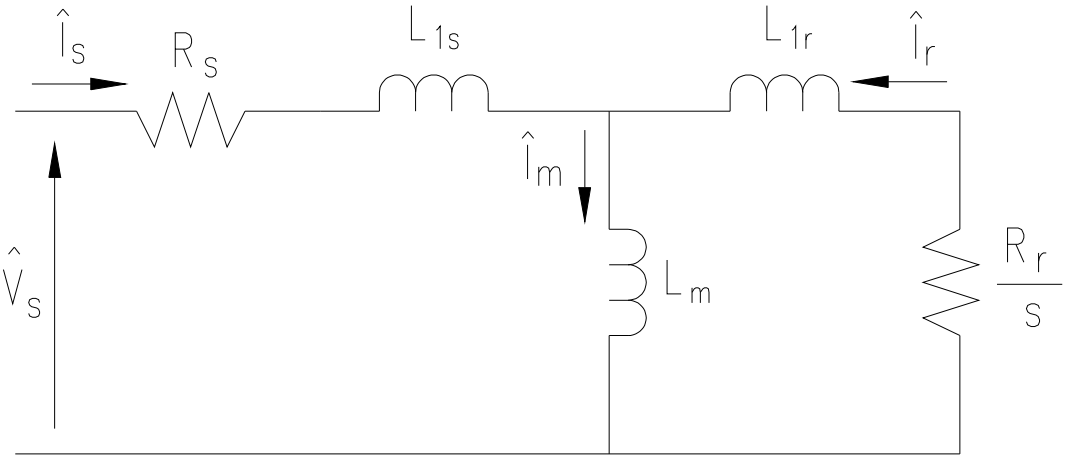

Figure 2.5. Steady-state equivalent circuit of an induction machine

stator leakage inductance and L_{1r} is the rotor leakage inductance and s is the slip. Two additional quantities, stator and rotor inductance, are now defined as:

$$L_s = L_{1s} + L_m \qquad \text{and} \qquad L_r = L_{1r} + L_m \tag{2.22}$$

Unlike synchronous machines, induction machines do not operate at synchronous speed. At rated speed, the speed of the rotor is slightly (2-7%) less than the synchronous speed. If the excitation frequency is ω and the actual rotor speed in electrical frequency unit is ω_r, then the slip is given as:

$$s = \frac{\omega - \omega_r}{\omega} = \frac{\omega_{sl}}{\omega} \tag{2.23}$$

where ω_{sl} is the rotor slip frequency. The electrical power transferred across the air gap from the stator is given as:

$$P_e = 3R_r \frac{\omega}{\omega_{sl}} I_r^2 \tag{2.24}$$

The developed torque, determined by subtracting the I^2R losses from electrical power and dividing the resultant power by the rotor speed, is given as:

$$T_e = 3P_p R_r \frac{I_r^2}{\omega_{sl}} \tag{2.25}$$

where P_p is the number of pole pairs.

Although traditional per phase equivalent circuit has been used in steady-state analysis, it is not appropriate for evaluation of dynamic performance of the induction machine [1]. Simply stated, it can not explain the dynamic performance of the induction machine. In order to understand and analyze the transient behavior of the induction machine, the dynamic equivalent circuit of the induction machine must be used.

The three-phase stator windings in an induction machine are designed to produce sinusoidal mmf in the space along the air-gap periphery. Assuming uniform air-gap and neglecting the effects of slot harmonics, the magnetic flux distribution will also be sinusoidal. For such machines the space vector transformation of section 2.4 can then be used. For a sinusoidal three-phase quantity, the corresponding space vector is a constant magnitude vector rotating at the angular speed, ω, imposed by the supply source. With space vector notation, voltage equations for the stator and rotor circuits of induction machine are given as [1]:

$$\hat{V}_s^s = R_s \hat{I}_s^s + \frac{d}{dt}\hat{\lambda}_s \tag{2.26}$$

and

$$\hat{V}_r^{'} = R_r^{'} \hat{I}_r^{'} + \frac{d}{dt}\hat{\lambda}_r = 0 \tag{2.27}$$

where $\hat{\lambda}_s$ is the stator flux, and $\hat{\lambda}_r$ is the rotor flux.

Just like in the steady-state equivalent circuit, it is very convenient to refer the rotor quantities to the stator. For that the $\frac{d}{dt}$ term must be replace by $\frac{d}{dt} - j\omega_r$ in the rotor equation. Hence,

$$0 = R_r^s \hat{I}_r^s + \left(\frac{d}{dt} - j\omega_r\right)\hat{\lambda}_r \tag{2.28}$$

where ω_r is the rotor angular speed in electrical frequency. The stator and rotor fluxes are related to the stator and rotor current as:

$$\begin{bmatrix} \hat{\lambda}_s \\ \hat{\lambda}_r \end{bmatrix} = \begin{bmatrix} L_s & L_m \\ L_m & L_r \end{bmatrix} \begin{bmatrix} \hat{I}_s \\ \hat{I}_r \end{bmatrix} \tag{2.29}$$

In algebraic form, the stator and rotor flux are given as:

$$\hat{\lambda}_s = L_s \hat{I}_s + L_m \hat{I}_r \tag{2.30}$$

and

$$\hat{\lambda}_r = L_m \hat{I}_s + L_r \hat{I}_r \tag{2.31}$$

Equations (2.26), (2.28) and (2.29) constitute the dynamic equivalent circuit of the induction machine on a stationary reference frame. Using equations (2.30) and (2.31), equations (2.26) and (2.28) can be represented as:

$$\hat{V}_s^s = R_s \hat{I}_s^s + L_s \frac{d}{dt}\hat{I}_s^s + L_m \frac{d}{dt}\hat{I}_r^s \tag{2.32}$$

and

$$0 = R_r \hat{I}_r^s + L_r \frac{d}{dt}\hat{I}_r^s + L_m \frac{d}{dt}\hat{I}_s^s - j\omega_r (L_r \hat{I}_r^s + L_m \hat{I}_s^s) \tag{2.33}$$

The dynamic equivalent circuit obtained from equations (2.32) and (2.33) is shown in Figure 2.6.

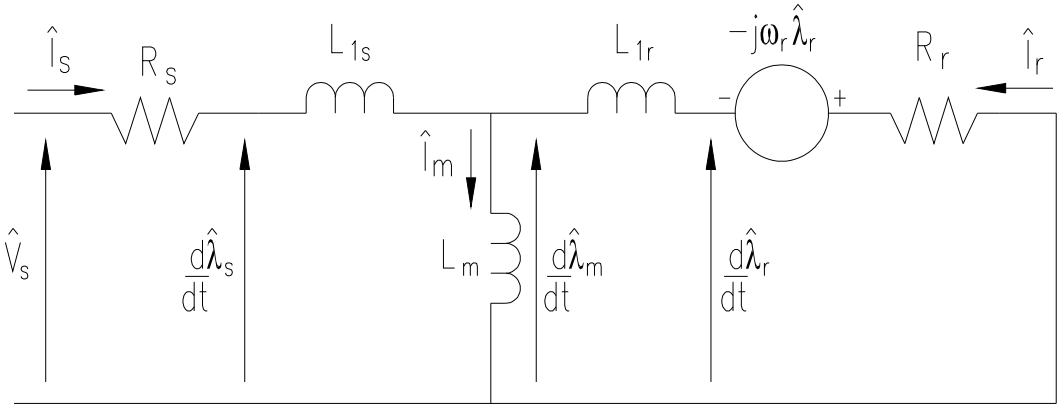

Figure 2.6. Dynamic equivalent circuit for a stator reference frame

Figure 2.7 shows an ideal induction machine. In steady-state, space vectors of motor variables revolve in the stator frame of reference with angular speed, ω, imposed by the supply source (inverter). It must be noted that this speed does not depend on the number of pole pairs, P_p. Under transient operating conditions, instantaneous speeds of the space vectors vary, and they are not necessarily the same for all vectors, but the vectors keep revolving nevertheless. Consequently, their *d* and *q* components are AC variables. Therefore, in addition to the static, three-phase to dq^s transformation (equation 2.6) and dq^s to three-phase transformation (equation 2.7), the dynamic, three-phase to *dq* can be represented in terms of the electrical angle, θ, between the rotor direct-axis and the stator phase a-axis as:

$$\begin{bmatrix} \Re_d \\ \Re_q \end{bmatrix} = \frac{2}{3}\begin{bmatrix} \cos\theta & \cos(\theta-120) & \cos(\theta+120) \\ -\sin\theta & -\sin(\theta-120) & -\sin(\theta+120) \end{bmatrix}\begin{bmatrix} \Re_a \\ \Re_b \\ \Re_c \end{bmatrix} \tag{2.34}$$

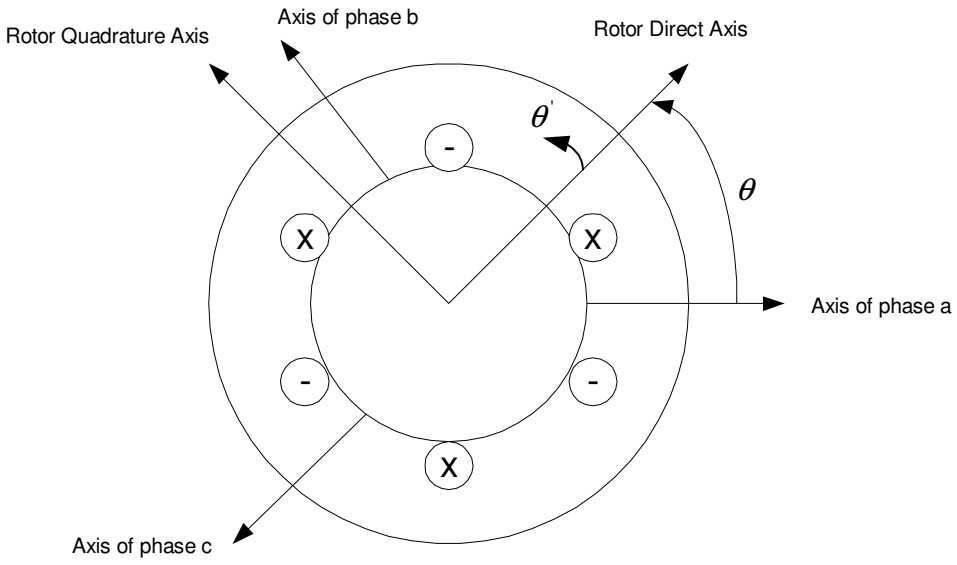

Figure 2.7. Ideal induction machine

Usually, a revolving reference frame is selected so that it moves in synchronism with a selected vector. The *d-q* components of the space vector in the revolving frame are now DC signals, constant in steady-state and varying in transient states. Considering the same space vector and a rotating *d-q* reference frame revolving at angular speed, ω_e, its stationary dq^s to rotating *dq* transformation can be written as:

$$\begin{bmatrix} \Re_d \\ \Re_q \end{bmatrix} = \begin{bmatrix} \cos(\omega_e t) & \sin(\omega_e t) \\ -\sin(\omega_e t) & \cos(\omega_e t) \end{bmatrix} \begin{bmatrix} \Re_d^s \\ \Re_q^s \end{bmatrix} \tag{2.35}$$

and the inverse, rotating *dq* to stationary dq^s transformation is given as:

$$\begin{bmatrix} \Re_d^s \\ \Re_q^s \end{bmatrix} = \begin{bmatrix} \cos(\omega_e t) & -\sin(\omega_e t) \\ \sin(\omega_e t) & \cos(\omega_e t) \end{bmatrix} \begin{bmatrix} \Re_d \\ \Re_q \end{bmatrix} \tag{2.36}$$

This transformation is known as Park Transformation [3].

The dynamic equivalent circuit of the induction machine for an arbitrary reference frame rotating at angular speed, ω_e, is now presented. Motor equations in a reference

frame rotating at ω_e can be obtained by replacing the $\frac{d}{dt}$ term by $\frac{d}{dt} + j\omega_e$ in equations 2.32 and 2.33 [1]. Thus:

$$\hat{V}_s^e = R_s \hat{I}_s^e + L_s\left(\frac{d}{dt} + j\omega_e\right)\hat{I}_s^e + L_m\left(\frac{d}{dt} + j\omega_e\right)\hat{I}_r^e \tag{2.37}$$

and

$$0 = R_r \hat{I}_r^e + L_r\left(\frac{d}{dt} + j\omega_e\right)\hat{I}_r^e + L_m\left(\frac{d}{dt} + j\omega_e\right)\hat{I}_s^e - j\omega_r(L_r\hat{I}_r^e + L_m\hat{I}_s^e) \tag{2.38}$$

where superscript *e* designates an arbitrary rotating frame.

The equations above can be simplified as:

$$\hat{V}_s^e = R_s\hat{I}_s^e + L_s\frac{d}{dt}\hat{I}_s^e + L_m\frac{d}{dt}\hat{I}_r^e + j\omega_e L_s\hat{I}_s^e + j\omega_e L_m\hat{I}_r^e$$

(2.39)

and

$$0 = R_r\hat{I}_r^e + L_r\frac{d}{dt}\hat{I}_r^e + +L_m\frac{d}{dt}\hat{I}_s^e + j(\omega_e - \omega_r)L_r\hat{I}_r^e + j(\omega_e - \omega_r)L_m\hat{I}_s^e \tag{2.40}$$

The new flux linkage terms are defined as:

$$\hat{\lambda}_s^e = L_s\hat{I}_s^e + L_m\hat{I}_r^e \tag{2.41}$$

and

$$\hat{\lambda}_r^e = L_m\hat{I}_s^e + L_r\hat{I}_r^e \tag{2.42}$$

The dynamic equivalent circuit of the induction machine for an arbitrary rotating reference frame is given in Figure 2.8.

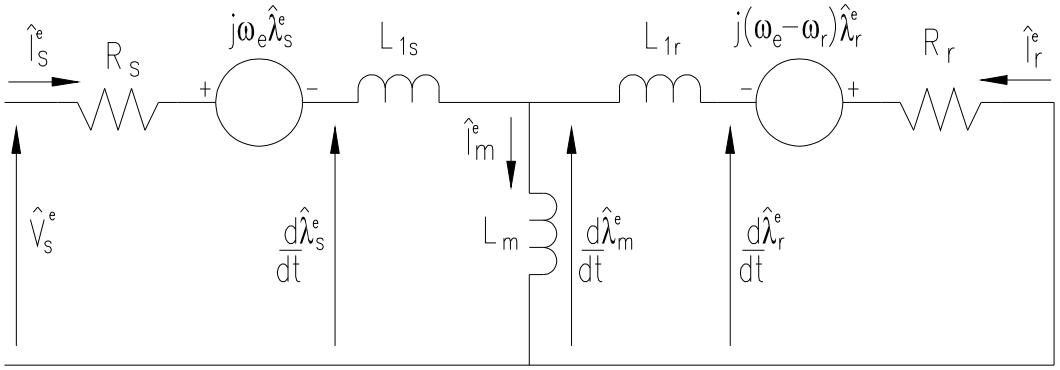

Figure 2.8. Dynamic equivalent circuit for an arbitrary rotating frame

Resolving the voltage and current space vectors into their respective *d-q* components, equations (2.39) and (2.40) can be expressed in matrix form as follows:

$$\begin{bmatrix} V_{ds}^e \\ V_{qs}^e \\ 0 \\ 0 \end{bmatrix} = \begin{bmatrix} R_s + L_s\frac{d}{dt} & -\omega_e L_s & L_m\frac{d}{dt} & -\omega_e L_m \\ \omega_e L_s & R_s + L_s\frac{d}{dt} & \omega_e L_m & L_m\frac{d}{dt} \\ L_m\frac{d}{dt} & -(\omega_e-\omega_r)L_m & R_r + L_r\frac{d}{dt} & -(\omega_e-\omega_r)L_r \\ (\omega_e-\omega_r)L_m & L_m\frac{d}{dt} & (\omega_e-\omega_r)L_r & R_r + L_r\frac{d}{dt} \end{bmatrix} \begin{bmatrix} I_{ds}^e \\ I_{qs}^e \\ I_{dr}^e \\ I_{qr}^e \end{bmatrix} \tag{2.43}$$

The equations for the stationary reference frame can also be obtained by simply substituting, $\omega_e = 0$ in equation (2.43) [10]:

$$\begin{bmatrix} V_{ds}^s \\ V_{qs}^s \\ 0 \\ 0 \end{bmatrix} = \begin{bmatrix} R_s + L_s\frac{d}{dt} & 0 & L_m\frac{d}{dt} & 0 \\ 0 & R_s + L_s\frac{d}{dt} & 0 & L_m\frac{d}{dt} \\ L_m\frac{d}{dt} & \omega_r L_m & R_r + L_r\frac{d}{dt} & \omega_r L_r \\ -\omega_r L_m & L_m\frac{d}{dt} & -\omega_r L_r & R_r + L_r\frac{d}{dt} \end{bmatrix} \begin{bmatrix} I_{ds}^s \\ I_{qs}^s \\ I_{dr}^s \\ I_{qr}^s \end{bmatrix} \tag{2.44}$$

For the *d-q* frame rotating at synchronous speed, ω, the dynamic equations are written in a matrix form as [13]:

$$\begin{bmatrix} V_{ds} \\ V_{qs} \\ 0 \\ 0 \end{bmatrix} = \begin{bmatrix} R_s + L_s \frac{d}{dt} & -\omega L_s & L_m \frac{d}{dt} & -\omega L_m \\ \omega L_s & R_s + L_s \frac{d}{dt} & \omega L_m & L_m \frac{d}{dt} \\ L_m \frac{d}{dt} & -\omega_{sl} L_m & R_r + L_r \frac{d}{dt} & -\omega_{sl} L_r \\ \omega_{sl} L_m & L_m \frac{d}{dt} & \omega_{sl} L_r & R_r + L_r \frac{d}{dt} \end{bmatrix} \begin{bmatrix} I_{ds} \\ I_{qs} \\ I_{dr} \\ I_{qr} \end{bmatrix} \tag{2.45}$$

where, $\omega_{sl} = \omega - \omega_r$, is the rotor electrical slip frequency. Based on equation (2.45), the *d-q* dynamic equivalent circuit for a synchronously rotating *d-q* frame can be created as shown in Figure 2.9. With the flux linkages defined as,

$$\lambda_{qs} = L_s I_{qs} + L_m I_{qr} \tag{2.46}$$

$$\lambda_{ds} = L_s I_{ds} + L_m I_{dr} \tag{2.47}$$

$$\lambda_{qr} = L_m I_{qs} + L_r I_{qr} \tag{2.48}$$

$$\lambda_{dr} = L_m I_{qs} + L_r I_{dr} \tag{2.49}$$

the induction machine dynamic equations are presented in the algebraic form as:

$$V_{qs} = R_s I_{qs} + \frac{d}{dt}\lambda_{qs} + \omega\lambda_{ds} \tag{2.50}$$

$$V_{ds} = R_s I_{ds} + \frac{d}{dt}\lambda_{ds} - \omega\lambda_{qs} \tag{2.51}$$

$$0 = R_r I_{qr} + \frac{d}{dt}\lambda_{qr} + \omega_{sl}\lambda_{dr} \tag{2.52}$$

$$0 = R_r I_{dr} + \frac{d}{dt}\lambda_{dr} + \omega_{sl}\lambda_{qr} \tag{2.53}$$

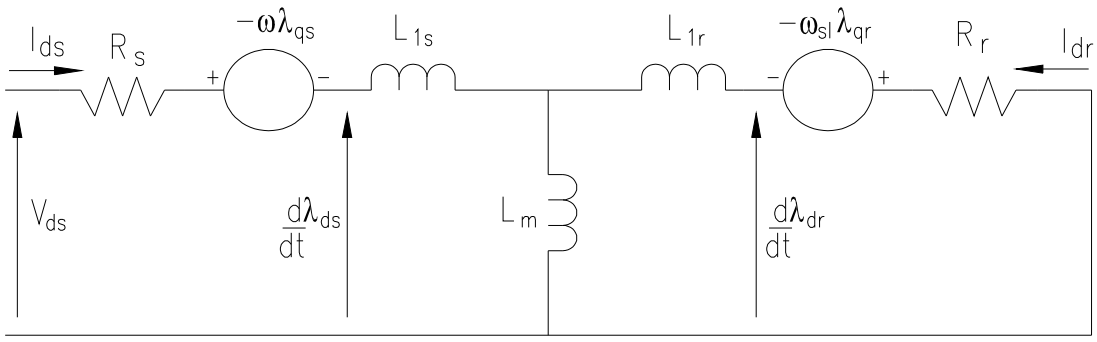

(a) d-axis Equivalent Circuit

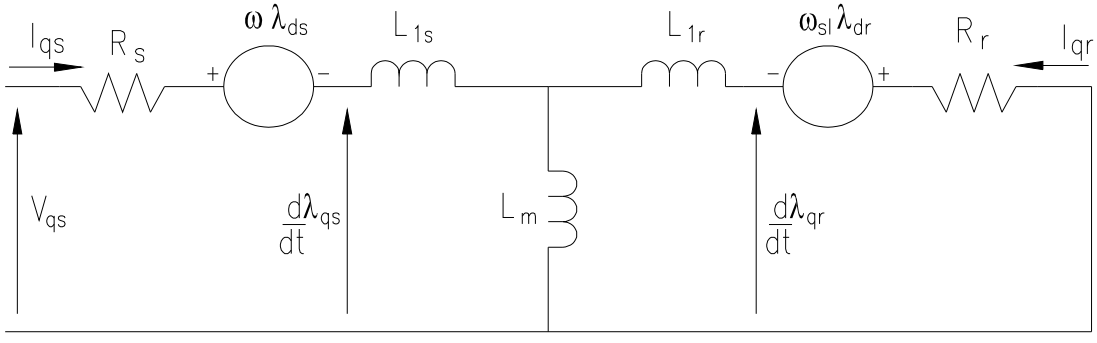

(b) q-axis Equivalent Circuit

Figure 2.9. *d-q* dynamic equivalent circuit for a synchronously rotating frame

The relationship between the *d-q* voltage components and the actual phase voltages is given as:

$$\begin{bmatrix} V_d \\ V_q \end{bmatrix} = \frac{2}{3}\begin{bmatrix} \cos\theta & \cos(\theta-120) & \cos(\theta+120) \\ -\sin\theta & -\sin(\theta-120) & -\sin(\theta+120) \end{bmatrix}\begin{bmatrix} V_a \\ V_b \\ V_c \end{bmatrix} \tag{2.54}$$

where V_a, V_b and V_c are the actual phase voltages at any give time, t.

The general expression for electrical power can be expressed as follows:

$$P_e = \frac{3}{2}\left(V_d I_d + V_q I_q\right) \tag{2.55}$$

The developed torque can be calculated in several forms as follows [1][2][13]:

$$T_e = \frac{3}{2} p_p \, \mathrm{Im}\{\hat{i}_s \, \hat{\lambda}_s^*\} = \frac{3}{2} p_p \left(i_{qs} \lambda_{ds} - i_{ds} \lambda_{qs} \right) \tag{2.56}$$

$$T_e = \frac{3}{2} p_p \frac{L_m}{L_r} \mathrm{Im}\{\hat{i}_s \, \hat{\lambda}_r^*\} = \frac{3}{2} p_p \frac{L_m}{L_r} \left(i_{qs} \lambda_{dr} - i_{ds} \lambda_{qr} \right) \tag{2.57}$$

or

$$T_e = \frac{3}{2} p_p L_m \, \mathrm{Im}\{\hat{i}_s \, \hat{i}_r^*\} = \frac{3}{2} p_p L_m \left(i_{qs} i_{dr} - i_{ds} i_{qr} \right) \tag{2.58}$$

It can be seen that the torque equations are all non-linear, and they include a difference of product of two motor variables.

The mechanical angular speed can be calculated from the torque equation as follows:

$$T_e - T_{load} - T_{fr} = J_{eff} \frac{d\omega_m}{dt} \tag{2.59}$$

where T_{load} is the load torque, T_{fr} represents the friction, J_{eff} is the total effective inertia, and ω_m is the rotor angular speed.

The rotor electrical speed, ω_r, can be determined from the rotor angular speed as:

$$\omega_r = P_p \omega_m \tag{2.60}$$

Equations (2.46) through (2.60) can be used to effectively model a squirrel cage induction machine in a simulation environment. In the next chapter, the vector control methods (field-oriented control) for the control of the induction machine are briefly presented. The dynamic equations are then adapted for a rotor field-oriented induction machine. Finally, an induction machine plant model consisting of the induction machine dynamic *d-q* model, voltage *d-q* transformation block and current inverse *d-q* transformation block is created.

3. INDUCTION MACHINE PLANT MODELING AND SIMULATION ENVIRONMENT

3.1. INTRODUCTION

In Chapter 2, the dynamic equations governing the behavior of induction machines were developed. As can be seen from the dynamic equations of the induction machine, its behavior is non-linear and thus requires a robust control scheme for controlling its torque and current response. In this chapter, the scalar and vector control schemes available for induction machines control, along with their advantages and disadvantages are briefly presented. Using the vector control scheme for induction machine control, the dynamic equations are obtained for a rotor field-oriented induction machine. Finally, a plant model consisting of the induction machine dynamic *d-q* model, the voltage *d-q* transformation block and current *d-q* inverse transformation block is created. The induction machine plant model is then used in a simulation environment using MATLAB-SIMULINK.

3.2. SCALAR CONTROLS

Of all the control schemes, scalar controls are perhaps the easiest and the simplest to accomplish. The two types of scalar controls are briefly described below.

3.2.1. Open-Loop Scalar Speed Control (constant V/Hz)

In this method, the approach is to approximately keep the stator flux constant in the machine regardless of the excitation frequency [18][20]. To maintain the flux at a constant rated level, the stator voltage is adjusted in proportion to the supply frequency. This is the simplest approach and is commonly referred to as constant volts/Hz method. This method also does not require any feedback. For low speed operation, the stator voltage drop across the stator resistance must be taken into account for maintaining constant flux. A user is typically required to input a stator voltage boost value during the initial commissioning of the variable frequency drive. At speeds above the base-speed, the motor operates in field-weakening region as the stator voltage can not be increased any further than the machine's rated voltage. Clearly, accurate speed control is not possible, because the actual slip varies with load and is not accounted for. In some control algorithms, a fixed value of slip at some load is added to the reference speed in order to achieve target speed. However, precision speed control is still not possible because slip variation is not taken into account. The open loop scalar control drives are still very popular and widely used in low-performance applications that do not require precision control such as pumps, fans, or grinders.

3.2.2. Closed-Loop Scalar Speed Control

In this scheme, the motor speed is monitored and compared with the reference speed by means of an encoder or other speed-measuring device. The speed error signal is applied to a PI type slip controller, which generates a new reference speed [20].

However, scalar controls only attempt to control the magnitude of the variables and thus are unable to provide fast dynamic control. With the advancement in vector control schemes, scalar closed-loop methods of speed control have now become obsolete [1].

3.3. VECTOR CONTROLS

Compared to scalar controls, which only involve controlling the magnitude of the control variables, a vector or field orientated control involves adjusting the magnitude and phase alignment of the vector quantities of the motor. Field-oriented control is the most popular high performance control technique for the AC induction machine. Progress in the field of power electronics has enabled the application of induction machines for high performance drives, where traditionally only DC motors were utilized [1]. With sophisticated control methods, AC induction drives offer the same control capabilities as high performance four-quadrant DC drives. The high performance AC drives allow vector control of the induction machine running in a closed loop with speed/position sensor providing the required feedback.

In the preceding chapter, the dynamic *d-q* equivalent circuit of the induction machine was presented. Using field-oriented control, the objective is to achieve de-coupled control of flux and torque so that a fast and accurate transient response can be achieved. The torque equation for the induction machine developed in the earlier chapter is given as:

$$T_e = \frac{3}{2} p_p \frac{L_m}{L_r} \mathrm{Im}\left\{\hat{i}_s \, \hat{\lambda}_r^*\right\} = \frac{3}{2} p_p \frac{L_m}{L_r} \left(i_{qs}\lambda_{dr} - i_{ds}\lambda_{qr}\right) \tag{3.1}$$

In the equation (3.1), if λ_{qr} were made equal to zero, then the torque equation would be similar to that of a DC machine. This situation is realized by aligning the direct-axis (*d*-axis) of the revolving *d-q* frame with rotor flux, λ_r. The *d-q* frame is now a revolving frame rotating at the synchronous speed, ω. This is shown in Figure 3.1. In this case, the electrical torque from equation (2.57) is given as:

$$T_e = \frac{3}{2} p_p \frac{L_m}{L_r} i_{qs} \lambda_{dr} \tag{3.2}$$

Similar results can be obtained by aligning the stator or air-gap flux with the *d*-axis of the *d-q* frame. The electrical torque for stator field alignment is given as [1]:

$$T_e = \frac{3}{2} p_p i_{qs} \lambda_{ds} \tag{3.3}$$

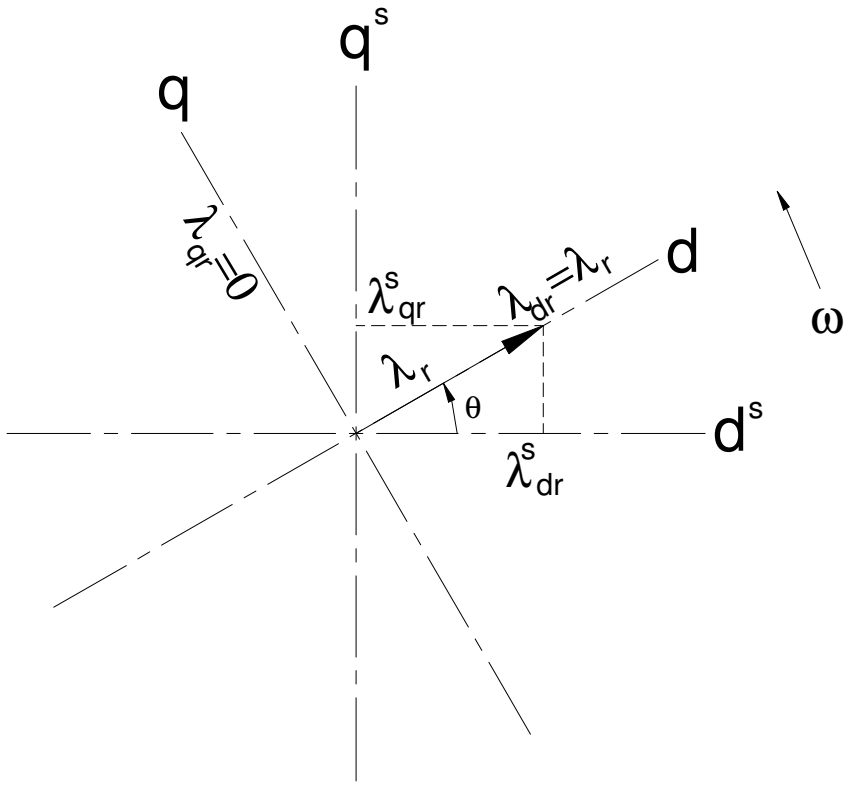

Figure 3.1. Alignment of *d-q* frame with rotor flux vector

The torque in a field-oriented control reacts instantly to changes in the I_{qs} component of stator current, and the reaction of rotor flux to changes in I_{ds} is inertial [1].

In summary, the principal of field-orientation requires that *d-q* frame must be aligned with a selected flux vector. For a given desired torque, $\overline{T}_e$, and desired flux vector, $\overline{\lambda}_f$, the desired currents, $\bar{I}_{ds}$ and $\bar{I}_{qs}$ are determined. Next, the angular position, θ_f, of the flux vector is determined and then used in the *d-q* transformation to obtain the respective three-phase phasors.

3.3.1. Direct Field-Orientation

In field-oriented control, the instantaneous position of the flux vector aligned with rotating *d-q* frame must be known at all times. The position of such a vector can be identified based on a direct measurement. In direct field-orientation, Hall Effect sensors of magnetic field are placed in the air-gap to measure the direct and quadrature component of the air-gap flux. Stator currents are measured as well. The rotor flux is then calculated as:

$$\hat{\lambda}_r = \frac{L_r}{L_m}\hat{\lambda}_m - L_{1s} I_s \tag{3.4}$$

However, these sensors are inconvenient, and require modifications to the induction machine in order to equip them. Furthermore, this spoils the ruggedness of the induction machine. For these reasons, indirect rotor field-orientation is most commonly used for vector control.

3.3.2. Indirect Field-Orientation

In the indirect field-orientation, the estimated angular position, $\overline{\theta}$, of the rotor flux vector is directly computed as:

$$\overline{\theta} = \int_0^t \overline{\omega}_{sl} dt + p_p \theta_m \tag{3.5}$$

where θ_m is the angular displacement of the rotor and $\overline{\omega}_{sl}$ is the required rotor slip frequency. Angular displacement, θ_m, is usually measured by a shaft position sensor such as a digital encoder. The required rotor slip frequency is computed as follows:

$$\overline{\omega}_{sl} = \frac{R_r}{L_r} L_m \frac{\bar{I}_{qs}}{\bar{\lambda}_r} \tag{3.6}$$

For indirect field-oriented control, the desired current $\bar{I}_{ds}$ can be found as follows:

$$\bar{I}_{ds} = \frac{1}{L_m}\left(\bar{\lambda}_r + \frac{L_r}{R_r} \frac{d}{dt} \bar{\lambda}_r \right) \tag{3.7}$$

In steady-state, $\frac{d}{dt}\bar{\lambda}_r = 0$, and $\bar{I}_{ds}$ is:

$$\bar{I}_{ds(steady\ state)} = \frac{\bar{\lambda}_r}{L_m} \tag{3.8}$$

The desired current, $\bar{I}_{qs}$, can be determined from the desired torque, $\overline{T}_e$, as:

$$\bar{I}_{qs} = \frac{2}{3P_p}\left(\frac{L_r}{L_m} \right) \frac{\overline{T}_e}{\bar{\lambda}_r} \tag{3.9}$$

The dynamic equations derived in Chapter 2 are repeated here for convenience. They are given as:

$$V_{qs} = R_s I_{qs} + \frac{d}{dt}\lambda_{qs} + \omega\lambda_{ds} \tag{3.10}$$

$$V_{ds} = R_s I_{ds} + \frac{d}{dt}\lambda_{ds} - \omega\lambda_{qs} \tag{3.11}$$

$$0 = R_r I_{qr} + \frac{d}{dt}\lambda_{qr} + \omega_{sl}\lambda_{dr} \tag{3.12}$$

$$0 = R_r I_{dr} + \frac{d}{dt}\lambda_{dr} + \omega_{sl}\lambda_{qr} \tag{3.13}$$

And the flux linkages are defined as:

$$\lambda_{qs} = L_s I_{qs} + L_m I_{qr} \tag{3.14}$$

$$\lambda_{ds} = L_s I_{ds} + L_m I_{dr} \tag{3.15}$$

$$\lambda_{qr} = L_m I_{qs} + L_r I_{qr} \tag{3.16}$$

$$\lambda_{dr} = L_m I_{ds} + L_r I_{dr} \tag{3.17}$$

For indirect field-orientation, $\lambda_{qr} = 0$, and $\lambda_{dr} = \lambda_r$, then equation (3.13) results in:

$$0 = R_r I_{dr} + \frac{d}{dt}\lambda_{dr} \tag{3.18}$$

Substituting I_{dr} from equation (3.17) into equation (3.18) results in:

$$0 = \frac{R_r}{L_r}\lambda_{dr} + \frac{d}{dt}\lambda_{dr} - \frac{R_r}{L_r}L_m I_{ds} \tag{3.19}$$

Using equations (3.16) and with $\lambda_{qr} = 0$:

$$I_{qr} = -\frac{L_m}{L_r} I_{qs} \tag{3.20}$$

Equation (3.12) can now be written as:

$$0 = -\frac{L_m}{L_r} R_r I_{qs} + \omega_{sl}\lambda_{dr} \tag{3.21}$$

Similarly, equations (3.10) and (3.11) can be rewritten for V_{ds} and V_{qs} as:

$$V_{qs} = R_s I_{qs} + \sigma L_s \frac{d}{dt} I_{qs} + \omega \sigma L_s I_{ds} + \frac{L_m}{L_r} \omega \lambda_{dr} \tag{3.22}$$

$$V_{ds} = R_s I_{ds} + \sigma L_s \frac{d}{dt} I_{ds} - \omega \sigma L_s I_{qs} + \frac{L_m}{L_r} \frac{d}{dt} \lambda_{dr} \tag{3.23}$$

where,

$$\sigma = 1 - \frac{L_m^2}{L_s L_r} \tag{3.24}$$

$$\lambda_{qs} = \sigma L_s I_{qs} \tag{3.25}$$

Equations (3.19), (3.21), (3.22) and (3.23) represent the dynamic voltage equations of the rotor field-oriented induction machine. It can be seen from the equations (3.2), and (3.19) that the stator component currents, I_{ds} and I_{qs}, of the rotating reference frame must be controlled to obtain de-coupled control of torque and rotor flux of the induction machine.

3.4. INDUCTION MACHINE PLANT MODEL

Figure 3.2 shows the simplified model of an indirect filed oriented induction machine system. This figure shows the basic blocks involved in the induction machine plant model. They are; "voltage *d-q* transformation block", "induction machine dynamic *d-q* model block", and "current inverse *d-q* transformation block".

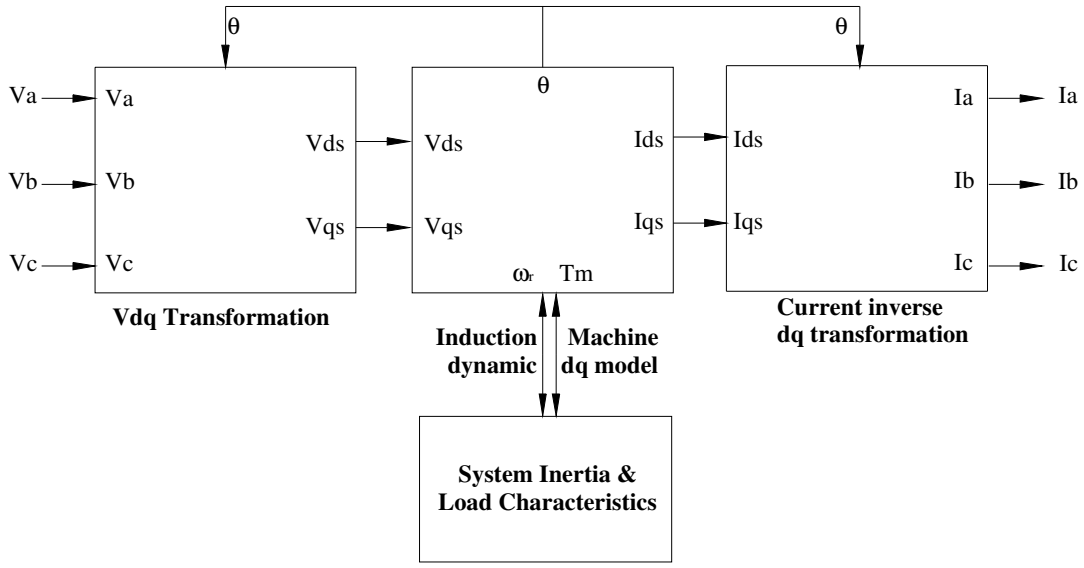

Figure 3.2. Block diagram of the induction machine plant

3.4.1. Voltage *d-q* Transformation Block

In an induction machine system, a controller issues the desired voltage commands for stator voltage components, $\overline{V}_{ds}$, and $\overline{V}_{qs}$ of the revolving frame, which are used to generate three-phase desired values. Using the three-phase desired voltages, the duty cycles needed to control the voltage source inverter are then calculated. Using the calculated duty cycles, and the pulse width modulated (PWM) technique, the voltage source inverter provides the input phase voltages, V_a, V_b, and V_c to the induction machine. This block utilizes the space vector transformations to convert the phase voltages V_a, V_b, and V_c in to the direct-axis voltage, V_{ds}, and quadrature-axis voltage, V_{qs}, of the rotating *d-q* frame. The transformations are performed according to the following equations:

$$\begin{bmatrix} V_{ds}^{s} \\ V_{qs}^{s} \end{bmatrix} = \begin{bmatrix} \frac{2}{3} & -\frac{1}{3} & -\frac{1}{3} \\ 0 & \frac{1}{\sqrt{3}} & -\frac{1}{\sqrt{3}} \end{bmatrix} \begin{bmatrix} V_a \\ V_b \\ V_c \end{bmatrix} \tag{3.26}$$

and

$$\begin{bmatrix} V_{ds} \\ V_{qs} \end{bmatrix} = \begin{bmatrix} \cos\theta & \sin\theta \\ -\sin\theta & \cos\theta \end{bmatrix} \begin{bmatrix} V_{ds}^{s} \\ V_{qs}^{s} \end{bmatrix} \tag{3.27}$$

The *d-q* voltage components are then provided as inputs to the "induction machine *d-q* model block". The rotor flux angular position, θ, needed for the phase voltage transformation into voltage *d-q* components, is computed in the "induction machine dynamic *d-q* model block".

3.4.2. Current Inverse *d-q* Transformation Block.

In this block, using space vector transformations shown in Chapter 2, the *d-q* current components, I_{ds} and I_{qs} of the revolving frame are inverse transformed to the three-phase AC currents. A current sensor is usually used to measure the three-phase currents of the induction machine, and provides current feedback to the controller. The inverse transformations are performed according to the following equations:

$$\begin{bmatrix} I_{ds}^{s} \\ I_{qs}^{s} \end{bmatrix} = \begin{bmatrix} \cos(\theta) & -\sin(\theta) \\ \sin(\theta) & \cos(\theta) \end{bmatrix} \begin{bmatrix} I_{ds} \\ I_{qs} \end{bmatrix} \tag{3.28}$$

and

$$\begin{bmatrix} I_a \\ I_b \\ I_c \end{bmatrix} = \begin{bmatrix} 1 & 0 \\ -\frac{1}{2} & \frac{\sqrt{3}}{2} \\ -\frac{1}{2} & -\frac{\sqrt{3}}{2} \end{bmatrix} \begin{bmatrix} I_{ds}^{s} \\ I_{qs}^{s} \end{bmatrix} \tag{3.29}$$

The rotor flux angular position, θ, needed for the *d-q* current transformation to three-phase currents, is computed in the "induction machine dynamic *d-q* model block" and used in the transformation block.

3.4.3. Induction Machine Dynamic *d-q* Model Block.

The direct-axis voltage, V_{ds} and quadrature-axis voltage, V_{qs} are provided as inputs to the "induction machine dynamic *d-q* model block". The dynamic equations of the indirect rotor field-oriented induction machine are implemented in this block to simulate the dynamic response of the induction machine. The outputs of the "induction machine dynamic *d-q* model block" are the direct-axis current, I_{ds}, quadrature-axis current, I_{qs}, rotor electrical angular speed, ω_r, and the rotor flux position, θ. Figure 3.3 shows the subset blocks involved that make up the "induction machine dynamic *d-q* model block".

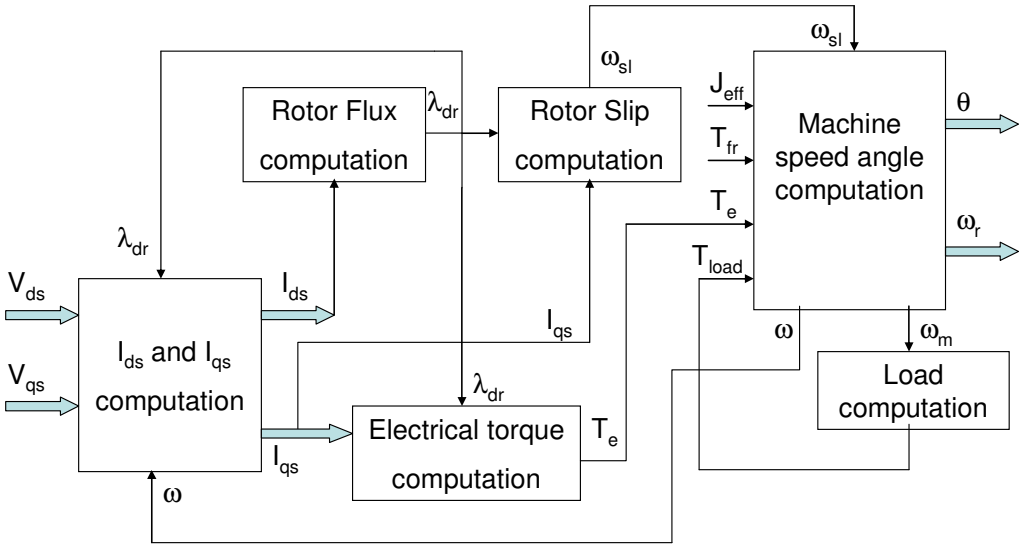

Figure 3.3. Block diagram of induction machine dynamic *d-q* model

3.4.3.1. I_{ds} and I_{qs} Computation

Figure 3.4 shows the block diagram of the I_{ds} and I_{qs} current computation block. In this block, the direct-axis voltages, V_{ds} and V_{qs}, are the inputs provided to the I_{ds} and I_{qs} computational block. The rotor flux λ_{dr} and synchronous speed, ω, which are determined in the rotor flux computation and the machine speed angle computation block respectively, provide the necessary feedback required to compute the direct-axis current, I_{ds}, and quadrature-axis current, I_{qs}.

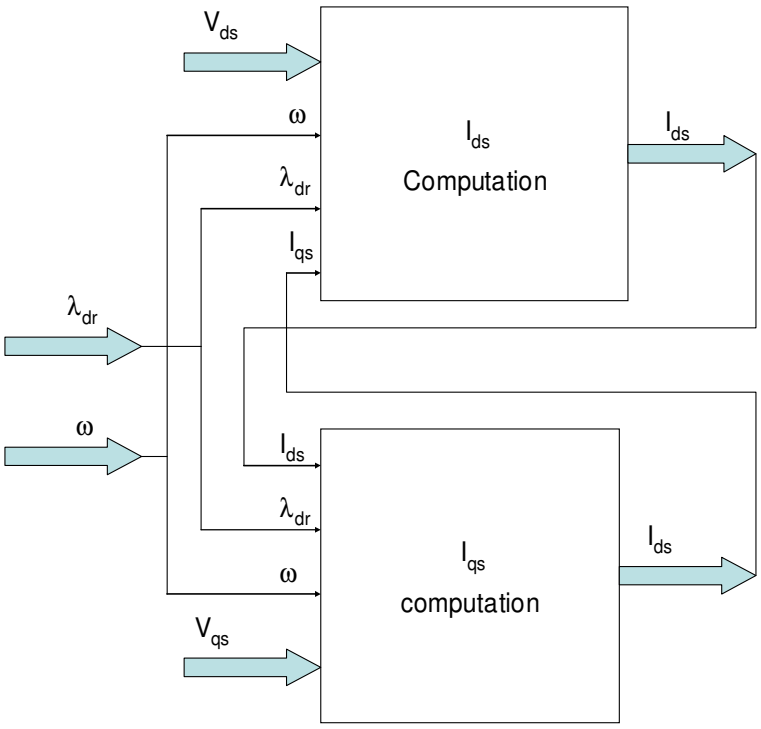

Figure 3.4. I_{ds} and I_{qs} computational block

The stator component currents, I_{ds} and $I_{qs,}$ of the revolving frame are calculated according to the following equations:

$$\sigma L_s \frac{d}{dt} I_{qs} = V_{qs} - R_s I_{qs} - \omega \sigma L_s I_{ds} - \frac{L_m}{L_r} \omega \lambda_{dr} \tag{3.30}$$

$$\sigma L_s \frac{d}{dt} I_{ds} = V_{ds} - R_s I_{ds} + \omega \sigma L_s I_{qs} - \frac{L_m}{L_r} \frac{d}{dt} \lambda_{dr} \tag{3.31}$$

where,

$$\sigma = 1 - \frac{L_m^2}{L_s L_r} \tag{3.32}$$

3.4.3.2. Rotor Flux Computation

In this block, the direct-axis current, I_{ds}, is used to compute the rotor flux. The rotor flux is computed as follows:

$$\frac{d}{dt}\lambda_{dr} = \frac{R_r}{L_r} L_m I_{ds} - \frac{R_r}{L_r}\lambda_{dr} \tag{3.33}$$

3.4.3.3. Rotor Slip Computation

The rotor flux, λ_{dr}, and quadrature-axis current, I_{qs}, are used to compute the rotor slip frequency. The computations are performed according to the following equation:

$$\omega_{sl} = \frac{L_m}{L_r \lambda_{dr}} R_r I_{qs} \tag{3.34}$$

3.4.3.4. Electrical Torque Computation

With the values of rotor flux, λ_{dr}, and quadrature-axis current, $I_{qs,}$ determined, the electrical torque is computed in this block according to the following equation:

$$T_e = \frac{3}{2} p_p \frac{L_m}{L_r} i_{qs} \lambda_{dr} \tag{3.35}$$

3.4.3.5. Load Computation

The load torque at the electric machine is needed to model the induction machine behavior. However, the ability to simulate various load conditions for the induction machine must be maintained. As an example, if one were to study the performance of

induction machines in hybrid or electric vehicles, the vehicle dynamic load would need to be modeled. Other applications of interest where a controlled induction machine dynamic behavior is desired are: elevator/hoist applications, spindle and servo applications and constant load applications. For this research, the load is modeled such that the robustness of the proposed controller under various situations, such as a step load torque change, and variable load torque can be studied. The following equation was used to model the load characteristics:

$$T_{load} = b_0 + b_1\omega_m + b_2\omega_m^2 \tag{3.36}$$

where b_o, b_1 and b_2 are constants, and ω_m is the rotor mechanical speed.

As can be seen from the equation above, by simply adjusting the values of the constants, the induction machine behavior can be studied for different load conditions using a single model.

3.4.3.6. Machine Speed Angle Computation

In this block, friction torque, T_{fr}, load torque, T_{load}, and effective system inertia, J_{eff}, are used to compute the rotor mechanical angular velocity, ω_m. The rotor electrical speed can be determined from the rotor mechanical speed by multiplying it with P_p poles pairs. The followings equations are used in this block to compute friction torque, T_{fr}, rotor mechanical angular velocity, ω_m, rotor electrical angular velocity, ω_r, synchronous speed, ω, and rotor flux position, θ:

$$T_e - T_{fr} - T_{load} = T_m - T_{load} = J_{eff}\frac{d\omega_m}{dt} \tag{3.37}$$

$$T_{fr} = k_f\omega_m + k_r\omega_m^2 \tag{3.38}$$

$$\omega_r = P_p \omega_m \tag{3.39}$$

$$\omega = \frac{d\theta}{dt} \tag{3.40}$$

$$\omega = \omega_{sl} + \omega_r \tag{3.41}$$

In equations (3.37) through (3.41), T_{load} is the load torque (Nm), T_{fr} represents the friction, k_f and k_r are the friction coefficients, T_m is the mechanical machine torque (Nm), J_{eff} is the total effective inertia (kg-m^2), ω_r is the electrical rotor speed (rad/s), ω_m is the rotor mechanical speed (rad/s), and θ is the electrical angular displacement of the rotor flux (rads).

3.5. ARCHITECTURE DEVELOPMENT

MATLAB-SIMULINK tools are used for model architecture development and simulations. This model is detailed enough that it can be used for evaluating the transient and steady-state response of the induction machine. Table 3.1 shows the technical specifications of the induction machine used for the plant model. For the purpose of the induction machine dynamics study and control system development, it is necessary to integrate the developed dynamic model with operator input, and an induction machine controller. In Chapter 4, a model of the induction machine controller that uses a fuzzy logic-based *d-q* control system to accurately control the dynamic response of the induction machine system is developed. In Chapter 5, through simulations, the performance of the proposed fuzzy controller is compared to that of the classical controller.

Table 3. 1. Technical specifications of the induction machine system

Parameter	**Value**
Rated Power	75 Hp
Rated speed	6000 r/min
Rated voltage	460V
Maximum speed	10000 r/min
No. of pole pairs	2
Stator Inductance, L_s	5.837 mH
Rotor Inductance, L_r	5.868 mH
Mutual inductance, L_m	5.650 mH
Stator resistance, R_s	0.0340 Ω
Rotor resistance, R_r	0.0227 Ω
Total effective inertia, J	0.0639 kg-m^2
Rotor flux at rated speed, λ_r	0.289 Wb

4. FUZZY LOGIC-BASED INDUCTION MACHINE CONTROL SYSTEM

4.1. INTRODUCTION

AC induction machines enjoy several advantages such as: ruggedness, simplicity, reliability, and low cost over DC machines. However, their control in high dynamic performance applications remains a challenge due to the non-linear model of the induction machine. Furthermore, motor parameters such as stator and rotor resistance, and mutual inductance vary with the operating conditions. Field-oriented control of the induction machine appears attractive, since under this scheme the de-coupling of the torque and flux is achieved. The de-coupling control method transforms the non-linear induction machine model to a set of linear equations, which can then be controlled by PI controllers. This method, however, greatly depends on the accurate mathematical model of the induction machine [5][4]. Conventional approaches use linear control algorithms to control the induction machine, which can result in undesired dynamic behavior. This issue arises from the fact that a complete high-fidelity mathematical model for the induction machine system, along with parametric variations cannot be accurately modeled inside the controller. Unfortunately, as a result of parameter changes and/or mismatches, the de-coupling of the torque and flux is not completely achieved. The dynamic performance of the induction machine then greatly deteriorates. Because of the non-linear nature of the induction machine, a highly robust control is needed to improve

the dynamic response of the induction machine. Therefore, a controller adaptable to non-linear behaviors and not requiring detailed knowledge of the mathematical model of the plant is required to address such issues [22].

The fuzzy logic-based induction machine controller, based on its non-linear approach, is an attractive choice which can accommodate the parameter variations of the induction machine. For a fuzzy logic controller, an accurate mathematical model of the induction machine is not required. Classical controllers with limitations have been used to control induction machines in achieving desired dynamic response. Fuzzy controls can provide a way to cope with the limitations of the classical controllers [13].

In this study, an innovative fuzzy logic-based *d-q* controller is presented, which improves the dynamic behavior of the induction machine when compared to the classical approach. This can improve two key attributes of the induction machine dynamic behavior; torque response and, I_{ds} and I_{qs}, current response. The objective of this work was to develop an induction machine control system with a non-linear controller using the fuzzy control paradigm to provide accurate control of I_{ds} and I_{qs} current under various transient conditions. The controller minimizes the stator currents, I_{ds} and I_{qs}, overshoots and undershoots and thus results in improved dynamic control of the torque and flux of the induction machine. Furthermore, this approach to current regulation would also mean that the torque response of the induction machine system could be optimized under dynamic conditions. The novel approach presented in this study uses a fuzzy logic-based *d-q* controller to determine output stator voltages commands based on the system's operating conditions.

4.2. SPEED AND TORQUE CONTROL OF INDUCTION MACHINE

A fuzzy logic-based induction machine controller must be able to provide two key attributes of the induction machine control. The attributes are speed control and torque control. Vector control techniques presented in Chapter 3 allow for speed and torque control of the induction machine in both the steady-state and transient operating conditions. Whether the induction machine system operates in speed control or torque control depends on the specific application. As an example, if the induction machine were to be used in an electric vehicle, the driver inputs (such as accelerator and brake pedal commands) would be considered torque commands and thus the controller would operate the induction machine in torque control mode. In the same way, when the electric vehicle is operated in cruise control, the controller provides speed regulation of the electric vehicle and subsequently controls the speed of the induction machine. In such a scenario, the induction machine operates in speed control mode.

4.2.1. Speed Control Based on Desired Speed

Figure 4.1 shows the system architecture from the perspective of induction machine speed control. The speed of the motor, ω_m, is usually determined as a time derivative of the rotor angle, θ_m. A very fast PI controller is then used, which compares the actual speed, $\omega_{m,}$ to the desired or reference speed and issues the torque command to achieve desired speed. Since a classical PI-type controller running at task rates of 100 μs or less with very aggressive proportional and integral terms are used, the error between desired induction machine speed and the actual machine speed is minimal. With such

accurate control of actual induction machine speed to the desired speed, the undesirable or objectionable (oscillatory) affects on induction machine speed are minimal and can be ignored.

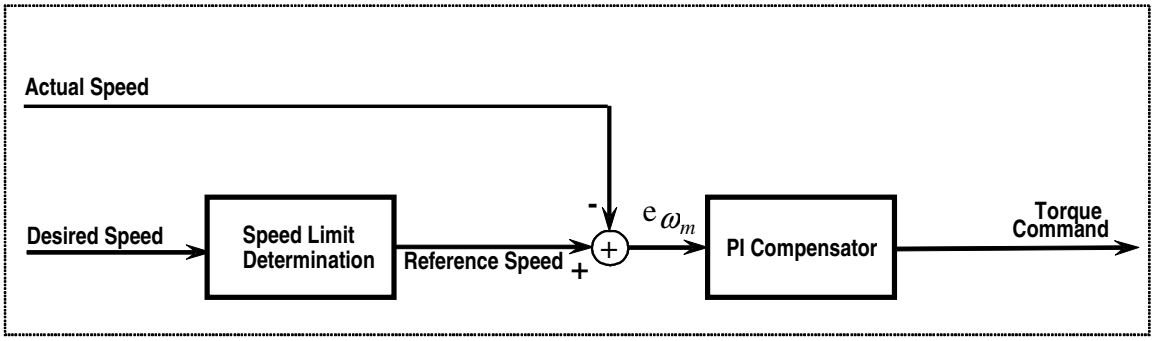

Figure 4.1. Induction machine speed control

4.2.2. Torque Control Based on Desired Torque

As mentioned earlier in Section 4.2, for a given torque demand (e.g. through accelerator and brake pedal requests in an electric vehicle) and machine operating conditions, the fuzzy logic-based induction machine control system commands the desired machine torque and maintains the optimal system dynamic response. Using field-oriented control methods, the controller achieves the independent control of torque and flux producing component of the stator current. Figure 4.2 shows the block diagram of an indirect field-oriented induction machine aligned with the rotor flux vector [1][3]. It is very clear from the block diagram of Figure 4.2 that in order to maintain a robust torque and rotor flux control, the direct-axis current, I_{ds}, and the quadrature-axis current, I_{qs}, of the rotating frame aligned with the rotor flux must be controlled.